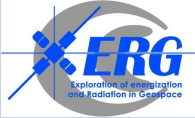


Multi-event analysis of STEVE, SAR arc, and red/green arc at subauroral latitudes using ground optical and radio instruments and the Arase and Van Allen Probes satellites



Rei Sugimura¹, Kazuo Shiokawa¹, Yuichi Otsuka¹, Shin-ichiro Oyama¹, Martin Connors², Akira Kadokura³, Alexey Poddelsky⁴, Igor Poddelsky⁴, Charles Smith⁵, Robert MacDowall⁶, Harlan Spence⁷, Geoff Reeves⁹, Herbert O. Funsten⁹, Yoshizumi Miyoshi¹, Iku Shinohara¹⁰, Yoshiya Kasahara¹¹, Fuminori Tsuchiya¹, Atsushi Kumamoto¹², Satoko Nakamura¹, Atsuki Shinbori¹, Kazushi Asamura¹³, Shoichiro Yokota¹⁴, Yoichi Kazama¹⁵, C.-W. Jun¹, Satoshi Kasahara¹⁷, Kunihiro Keika¹⁸, Tomoaki Hori¹, Ayako Matsuoka¹⁰, Nozomu Nishitani¹, Simon G. Shepherd⁵, John Michael Ruohoniemi⁶

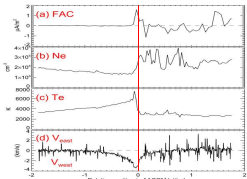
1. Institute for Space-Earth Environmental Research (ISEE), Nagoya University, 2. Athabasca University, 3. National Institute of Polar Research, Midori-cho 10-3, Tachikawa, Tokyo 190-8518, Japan, 4. Institute of Cosmophysical Research and Radiowave Propagation, Far Eastern Branch of the Russian Academy of Sciences, 5. Thayer School of Engineering, Dartmouth College, Hanover, NH, USA, 6. Bradley Department of Electrical and Computer Engineering, Virginia Tech, Blacksburg, VA, USA, 7. Institute for the Study of Earth, Oceans, and Space, University of New Hampshire, 8. NASA Goddard Space Flight Center, Greenbelt, MD, USA, 9. Los Alamos National Laboratory, Los Alamos, NM, USA, 10. Institute of Space and Astronautical Science, Japan Aerospace Exploration Agency, 11. Graduate School of Natural Science and Technology, Kanazawa University, 12. Graduate School of Science, Tohoku University, 13. Japan Aerospace Exploration Agency, 14. Department of Earth and Space Science, Graduate School of Science, Osaka University, 15. Academia Sinica Institute of Astronomy and Astrophysics, 16. Institute of Space and Plasma Sciences, National Cheng Kung University, 17. Department of Earth and Planetary Science, School of Science, University of Tokyo, 18. Graduate School of Science, Tokyo University



1. Introduction

Strong Thermal Emission Velocity Enhancement (STEVE)

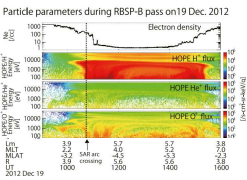
- Atmospheric optical phenomenon that appears with purple emission and observed above picket-fence (green emission). (MacDonald et al., 2018)
- Wide spectrum from 400 to 730 nm (Gillies et al., 2019)
- Optical manifestations associated with SAID in the ionosphere (Chu et al., 2019)



STEVE

Stable Auroral Red (SAR) arc

- 630 nm (red) emission of oxygen atoms at subauroral latitudes
- The SAR arc is caused by Coulomb collisions between cold electrons in the plasmasphere and hot ions in the ring current. (Inaba et al., 2021)



SAR arc

Red and Green arc

- Arc with red and green emission (Red and green arc) have also been reported. (Mendillo et al., 2016)

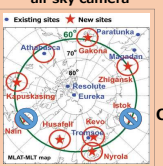
For the first time we analyzed multiple cases of STEVE, SAR arc, red and green arcs, an unprecedented number of conjugate events (9 events), and compared the characteristics of magnetospheric plasma and electromagnetic field variation.

2. Instrumentation

Ground

OMTI's high-sensitivity all-sky camera

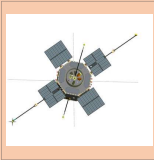
SuperDARN



Magnetosphere

Van Allen Probes (RBSP)

ERG



Shiokawa et al. (2017)

Nishitani et al. (2019)

HOPE, EMFISIS
Miyoshi et al. (2012)

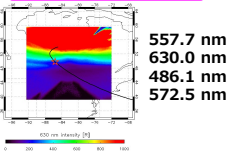
PWE, MEP-I, LEP-I, MEP-e, LEP-e, EFD, MGF

4. Results & discussion

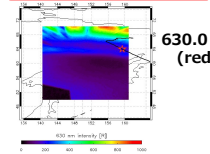
Events analyzed in this study

NUM	STA	TIME	DAY	TYPE	SATELLITE
1	KAP	00:57~04:20(UT)	2017/3/22	STEVE	RBS-P-B
2	KAP	02:21~04:47(UT)	2017/8/20	STEVE	ERG
3	KAP	03:11~03:41(UT)	2018/9/14	STEVE	RBS-P-B
4	MGD	10:45~15:15(UT)	2017/3/27	SAR arc	RBS-P-A
5	GAK	6:03~8:48(UT)	2020/1/16	SAR arc	ERG
6	ATH	3:53~8:10(UT)	2021/1/12	SAR arc	ERG
7	ATH	04:45~07:01(UT)	2017/2/17	RED/GREEN ARC	RBS-P-B
8	ATH	05:25~07:57(UT)	2018/2/17	RED/GREEN ARC	RBS-P-B
9	GAK	3:30~7:20(UT)	2019/2/2	RED/GREEN ARC	RBS-P-A

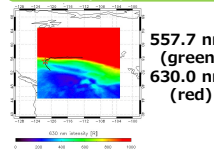
STEVE on 2017/03/22 at KAP



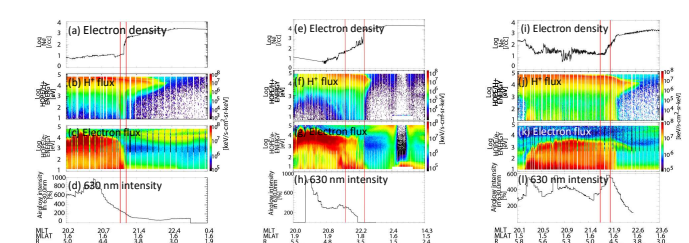
SAR arc on 2017/03/27 at MGD



Red and Green arc on 2017/02/17 at ATH



Comparing energy flux data obtained from the satellites

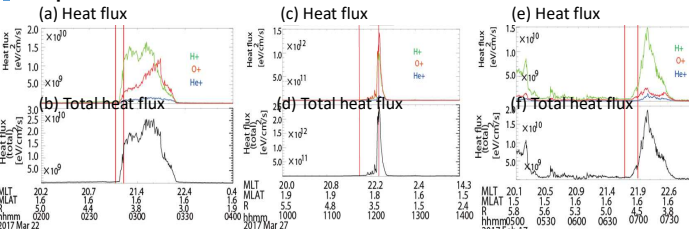


The arcs occur in the overlap region of the plasmasphere boundary and the ring current.

The electron energy rises at the arc crossing.

No clear difference in particle energy or electron density for these three arcs.

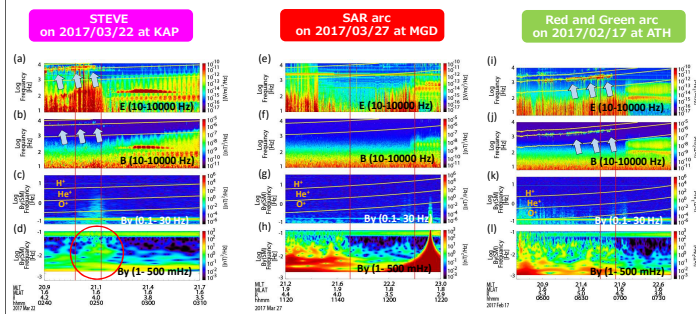
Comparison of heat flux



Despite the SAR arc having the weakest airglow intensity, the heat flux is the highest.

The STEVE and red/green arcs emit light due to factors other than Coulomb collisions.

Comparing electromagnetic waves obtained from the satellites

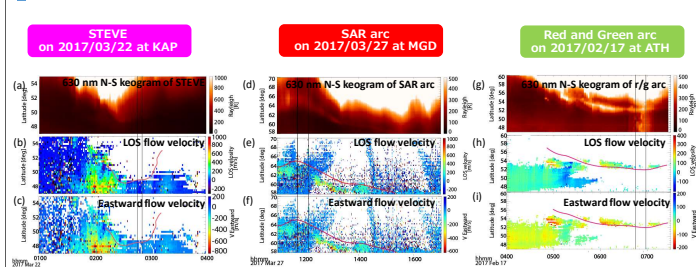


Chorus waves are observed during a STEVE and a red/green arc.

The magnetic waves at ~0.001~0.1 Hz are observed during a STEVE.

The emission of 557.7 nm is generated by high-energy electron precipitation scattered by pitch angle due to wave-particle interactions.

Comparing plasma flow obtained from the SuperDARN radar



Westward plasma flow (STEVE: ~600 m/s, SAR arc: ~200 m/s, red and green arc: ~100 m/s) occurs along the arc.

5. Conclusions

We analyzed 9 conjugate observations of STEVE, SAR, red/green using 3 magnetospheric satellites and 7 ground-based all-sky cameras over a four-year period from January 2017 to April 2021.

Most of the three types of arcs (8/9) had similar source features that their source is in the overlap region between the plasmapause and the ring current.

Heat fluxes are higher for the SAR arc than for the STEVE and the red/green arc.

The Chorus waves were observed only in STEVE (3/3) and Red and green arc (3/3) events.

SuperDARN data showed a strong westward flow in the ionosphere during the STEVE event.

- Under conditions of SAR arc generation
 - Electromagnetic wave occurs → Red/green arc
 - Strong westward flow occurs → STEVE